Review

Surface-enhanced infrared absorption spectroscopy (SEIRAS) to probe monolayers of membrane proteins ☆

Kenichi Ataka, Sven Timo Stripp, Joachim Heberle *

Freie Universität Berlin, Experimental Molecular Biophysics, Arnimallee 14, 14195 Berlin, Germany

ABSTRACT

Surface-enhanced infrared absorption spectroscopy (SEIRAS) represents a variation of conventional infrared spectroscopy and exploits the signal enhancement exerted by the plasmon resonance of nano-structured metal thin films. The surface enhancement decays in about 10 nm with the distance from the surface and is, thus, perfectly suited to selectively probe monolayers of biomembranes. Peculiar to membrane proteins is their vectorial functionality, the probing of which requires proper orientation within the membrane. To this end, the metal surface used in SEIRAS is chemically modified to generate an oriented membrane protein film. Monolayers of uniformly oriented membrane proteins are formed by tethering His-tagged proteins to a nickel nitrilo-triacetic acid (Ni-NTA) modified gold surface and SEIRAS commands molecular sensitivity to probe each step of surface modification. The solid surface used as plasmonic substrate for SEIRAS, can also be employed as an electrode to investigate systems where electron transfer reactions are relevant, like e.g. cytochrome c oxidase or plant-type photosystems. Furthermore, the interaction of these membrane proteins with water-soluble proteins, like cytochrome c or hydrogenase, is studied on the molecular level by SEIRAS. The impact of the membrane potential on protein functionality is verified by monitoring light–dark difference spectra of a monolayer of sensory rhodopsin (SRII) at different applied potentials. It is demonstrated that the interpretations of all of these experiments critically depend on the orientation of the solid-supported membrane protein. Finally, future directions of SEIRAS including cellular systems are discussed. This article is part of a Special Issue entitled: FTIR in membrane proteins and peptide studies.

© 2013 Elsevier B.V. All rights reserved.

Contents

1. Introduction

The composition of amino acids at the surface of a protein determines whether it is water soluble or not. While the majority of proteins are found with a predominantly hydrophilic surface, polypeptides that interact with lipid membranes have large hydrophobic areas. For example, transmembrane proteins are dissolved in the lipid bilayer and allow for hydrophilic interactions only where the protein pokes out of the membrane. Similar to the importance of the solvation shell for soluble proteins in terms of structural integrity and function, membrane proteins do not fold into their tertiary or quaternary structures and lack any activity in the absence of a lipidic environment. Therefore, meaningful biophysical studies on membrane proteins involve the reconstitution of detergent-purified protein into a lipid bilayer. Such biomimetic membranes should provide the following essential features: i) the protein molecules are arranged to form a monolayer immersed in a bilayer of lipids, ii) the vectorial functionality requires strict orientation of the membrane protein within the lipid layer, and iii) a membrane potential must be applicable. These minimal conditions are considered crucial for meaningful investigations of the functional mechanism of membrane proteins. Such is the challenge for functional investigations of membrane proteins by Fourier-Transform Infrared (FTIR) spectroscopy which has been demonstrated to be a valuable tool to study transmembrane proteins [1–4] as well as membrane-associated proteins [5].

The detection of the absorption from a protein monolayer by conventional transmission FTIR spectroscopy is challenging due to the low signal strength. A monolayer typically corresponds to a few pico mol protein per cm^2. The 'surface enhancement effect' when introduced to IR absorption spectroscopy (the technique commonly referred to as Surface Enhanced Infrared Absorption Spectroscopy, SEIRAS) [6] leads to the increase of signal intensity by two orders of magnitude. As the plasmonic field of the metal surface significantly contributes to the mechanism of enhancement, the effective range of signal enhancement is restricted to the immediate vicinity of the surface (<10 nm) [7]. Thus, a protein monolayer is probed by molecular spectroscopy with the sample adsorbed to a SEIRA-active metal film surface. Solid-supported protein monolayers attract growing research interest as the basis of bio-nano devices [8]. Protein monolayers can be generated by controlled adsorption on the solid surface by various approaches. Solid-supported membrane proteins represent good and stable model system for cell membranes and membrane potentials can be applied by exploiting the supporting metal surface as an electrode. This article reviews the methodology and presents recent developments in the application of SEIRAS to membrane proteins.

2. Methodology

2.1. Basic principles of surface enhanced IR absorption spectroscopy

Surface enhancement along rough metal surfaces arises from local electromagnetic (EM) field enhancement through excitation of Surface Plasmon Polaritons (SPP) [7,9]. A ten-fold stronger EM field was calculated to contribute to the overall surface enhancement [10]. The local EM field intensity decays sharply with the distance from the surface (on the order of 10 nm). The EM mechanism is usually used to explain the near-field effect of SEIRAS. However, the demodulation of absorption by the metal/adsorbate layer (mixed effective medium) is considered to play an equally important role in the mechanism of enhancement [7]. The dielectric properties of the metal film are altered when dipoles of adsorbed molecules induce mirror dipoles in the metal substrate. The effect is large at frequencies of IR absorption of the adsorbed molecule, i.e. in the mid-IR frequency range (typically 4000–400 cm^{-1}). The vibrational contribution of adsorbed molecules induces a change in the transmittance or reflectance of the metal film. It should be noted that the

absorption coefficients of metals are larger than those of organic compounds and the metal volume is much larger than that of the adsorbed molecules. Consequently, changes in the optical properties of the metal film will dominate the spectrum.

The topology of the metal surface significantly contributes to the enhancement properties. Typically, nano meter scale of -roughened surfaces are used. Since the average distance between metal particles at a given roughness is much smaller than the wavelength of IR radiation, the optical properties of the metal film are assumed to arise from a mixed composition of metal, adsorbed molecules, and surrounding host medium. By modeling a dielectric of such composite layer, one can estimate a contribution from the enhancement factor of the mixed effective medium. The dielectric function of the composite layer, ε_{BR}, is given by the Bruggeman effective medium theory:

$$\varepsilon_{BR} = \varepsilon_h \frac{3(1-F)+F\alpha}{3(1-F)-2F\alpha} \tag{1}$$

where F is the packing density of the metal in the composite layer, ε_h is the dielectric function of the host medium (e.g., water), and α is the polarizability of a metal particle. The value of α is highly dependent on the shape of the metal particle and the polarization of the incident light, as given by the following equation:

$$\alpha_{\perp,\parallel} = \left\{ \frac{(\varepsilon_d-\varepsilon_h)[\varepsilon_m L_1+\varepsilon_d(1-L_1)]+Q(\varepsilon_m-\varepsilon_d)[\varepsilon_d(1-L_2)+\varepsilon_h L_2]}{[\varepsilon_d L_2+\varepsilon_h(1-L_2)][\varepsilon_m L_1+\varepsilon_d(1-L_1)]+Q(\varepsilon_m-\varepsilon_d)(\varepsilon_d-\varepsilon_h)L_2(1-L_2)} \right\}_{\perp,\parallel} \tag{2}$$

where subscripts $\perp$ and $\parallel$ refer to the polarization of the radiation being perpendicular (p-polarized, in reflection configuration) and parallel (s-polarized) with respect to the substrate surface. ε_d and ε_m are the dielectric constants of the adsorbed molecule and the metal, respectively. Since ellipsoid is assumed for the shape of the metal particle, L is the depolarization factor of the ellipsoid given as a function of the aspect ratio of the ellipsoid and is normalized to $L_\perp + 2L_\parallel = 1$. The subscripts of L (1 and 2) refer to the value of core (metal particle) and coated (metal particle + adsorbed molecules) ellipsoids, respectively. Q is the volume ratio of the core and coated ellipsoids ($Q = V_1/V_2$). Thus, the thickness of the molecular layer can be varied through Q.

Inserting the topographical sizes of the Au particle and the molecular dielectric into these equations, Osawa simulated the enhanced spectrum recorded at various optical configurations [7,11,12] and calculated an enhancement factor of 30. If the plasmonic EM field enhancement (about 10-fold, vide supra) is taken into account, the theoretical enhancement factor of 300 agrees well with the experimentally determined enhancement factor of several hundreds [7].

The polarization α critically depends on the polarization of incident light (Eq. (2)). When the polarization is changed from p to s, the enhancement is decreased to 1/5 [13]. In the actual experiment, the intensity of the SEIRA spectrum of 2-anthraquionecarboxylic acid is reduced by 1/20 upon the change from perpendicular to parallel polarization. Despite the quantitative difference in the enhancement factor between the observed and simulated spectra, these results clearly demonstrate that SEIRAS exhibits strong polarization dependence.

An important feature of SEIRAS is the so-called surface selection rule. Vibrational bands that arise from a change in dipole moment parallel to the surface normal are strongly enhanced while those comprising a perpendicular component are weakened. Obeying the surface selection rule, some bands may appear with different intensities in the SEIRA spectrum as compared to the conventional IR spectrum. The surface selection rule can be exploited to determine the surface orientation of adsorbed molecules by comparing relative intensities between bands of orthogonal dipole moment vectors [6,7].

The polarization α is also highly dependent on the shape of the metal particle. It was shown [11] that the enhancement is stronger

as the lateral axis gets longer then the longitudinal axis. This prediction was confirmed experimentally by using extremely elongated shaped nano-particle, such as gold nano-rods [14]. It was recently reported that a periodic array of silver nano-rods generate a signal enhancement in the order of 10^4–10^5 [15]. Such super enhancement allow for probing adsorbates down to zeptomole concentrations (10^{-21} M) by IR spectroscopy.

Another advantage of SEIRAS is the fact that the strived enrichment of sample along the solid surface reduces the content of water in the observed volume as the strong absorption of liquid water often hampers the IR spectroscopic analysis. In Attenuated Total Reflection (ATR) configuration (Fig. 1(a)), only those molecules are probed that reside within the optical near-field of the SPP (about 10 nm, vide infra) because the incident IR radiation does not traverse the solution before reaching the plasmonic surface. Rather, a single-reflection trapezoidal silicon (Si) prism is used as internal reflection element. The probing IR beam irradiates the backside of the prism at an incident angle of 60°. The beam is totally reflected at the surface of the Si prism where a rough gold thin film (20–200 nm thickness) was formed by chemical or by vapor deposition. Additional advantages of the internal reflection configuration are that the probing IR beam is protected from atmospheric absorption and that the plasmonic gold film is accessible to manipulation during the experiments.

It is interesting to discuss the technical merits of SEIRAS in comparison to other IR methods. An early approach for detection of monolayers at the solid/liquid interface is Infrared Reflection Absorption Spectroscopy (IRRAS, Fig. 1(b)) [16]. The IR beam is directed through a prism with a low-refractive index material such as CaF_2 or BaF_2. The incident IR beam passes the solution and is reflected at the metal surface on which the molecular monolayer has been formed atop. The absorption of the monolayer is enhanced five to ten times when the grazing angle of the incident beam is chosen [17]. To minimize the optical path through the solution, the metal surface is mounted in μm distance to the prism. The IR absorption of the solution is usually much stronger than the contribution of the monolayer. Investigations of biological systems are strongly hampered by the H–O–H bending mode of liquid water (around 1650 cm^{-1}) that overlaps with many important bands of the monolayer under study. The strong overlap with the amide I band of the peptide backbone renders secondary structure analysis of proteins in water difficult. Consequently, IRRAS has typically employed for studies in the spectral region >1800 cm^{-1} (analysis of carbon monoxide or cyanide bands [18,19]). Furthermore, H_2O can be exchanged for deuterium oxide (D_2O) to shift the bending mode to lower frequencies. Minimizing the optical path could be an option but comprises another disadvantage. Since the gap is designed extremely thin, diffusion of reaction species to the monolayer is hampered. This becomes problematic for functional studies of enzymes that are driven by the availability of reactants and concentration of products. Insufficient reactant concentrations or product holdup can diminish catalytic activity, inhibit, or even reverse the reaction.

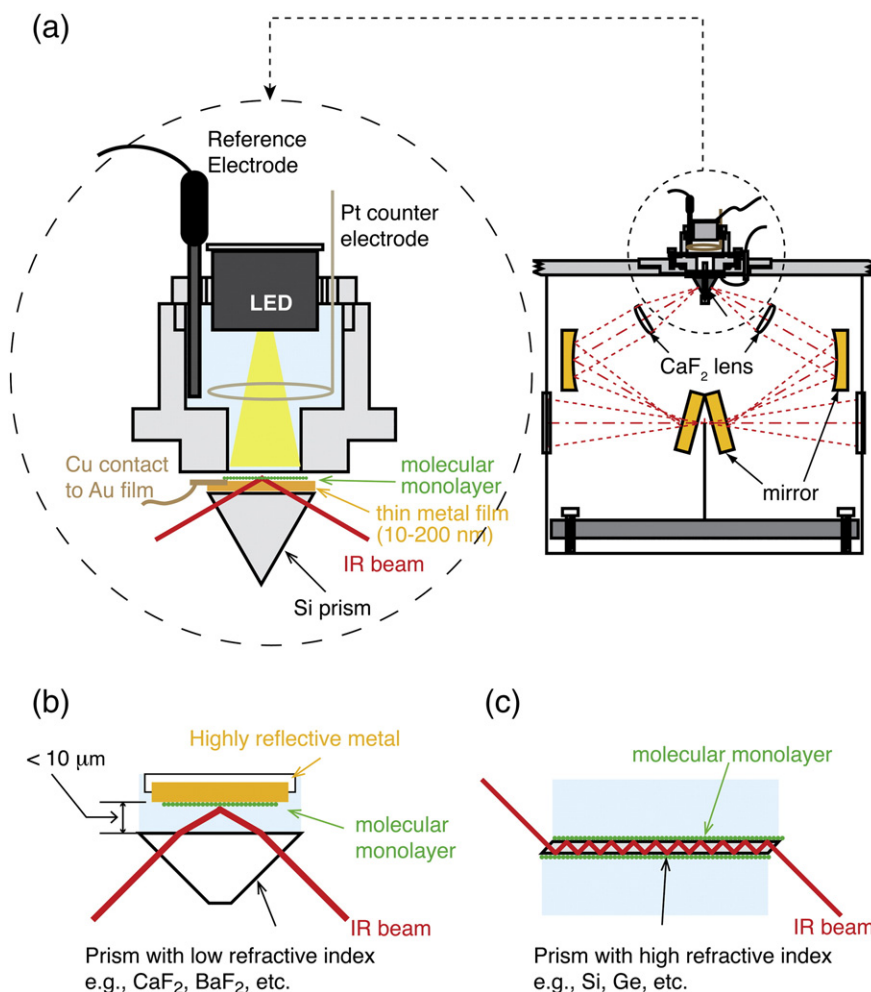**Fig. 1.** (a) Sketch of the experimental setup for Surface Enhanced Infrared Absorption Spectroscopy (SEIRAS) with the prism for attenuated total reflection (right) and the spectro-electrochemical cell with LED for illumination (left). (b) Optical setup for Infrared Reflection Absorption Spectroscopy (IRRAS). (c) Conventional attenuated total reflection unit with multiple internal reflections.

The ATR technique provides sufficient sensitivity to detect a monolayer even in the absence of surface enhancement. In this case, the number of reflections can be raised to typically 20 (Fig. 1(c)) [20–22]. Signal intensity increases with each reflection but the probing beam amplitude is diminished as well. Therefore, strong IR sources are required to allow for an appropriate signal-to-noise ratio and meaningful difference spectra. Besides optical difficulties, a major drawback is the fact that vibrational contributions from the solvent increase concomitantly with the monolayer signal.

2.2. Immobilization of proteins to solid surfaces

The choice of an appropriate immobilization method is key to address the functionality of a membrane protein monolayer. Immobilization of membrane proteins on solid supports is intrinsically more difficult than to adhere water soluble proteins. The amphiphilic character of membrane proteins and their low conformational stability easily influences their properties through interaction with the solid surface. Proteins can adsorb to surfaces by a variety of interactions such as electrostatic attraction, hydrogen bonding, hydrophobic interaction, etc. As energies are weak, the diversity of these interactions often leads to non-specific binding which is unfavorable for functional studies. One of the major challenges in protein immobilization is to control the orientation of proteins and retain biological activity at the same time.

Chemical modification involves coating of the solid surface by organic molecules that specifically enhance the affinity to proteins and that prevent undesired interactions with the surface itself. These so-called Self-assembled Monolayers (SAMs) are commonly exploited due to facile preparation and their plasticity regarding chemical structure and functionality. The SAM method makes use of molecules that spontaneously form a monolayer when exposed to the solid surface. Three functional domains characterize a SAM-forming molecule: (i) The terminal head often consists of thiol (-SH or disulfide (-SS-) groups that allow for covalent bonding to the metal support (typically gold or silver). (ii) The backbone consists of an alkyl chain of variable length (C_1–C_{12}). This un-reactive spacer provides a flexible cushion for tethered proteins. (iii) At the other end, the molecule is terminated by a group which enables direct and specific interaction with the protein of choice. If the functional group is polar (-OH, -COOH, -NH_2, etc.), an electrostatic interaction with charged regions of the target protein can be established. The oriented adsorption by this strategy works well with small-sized water-soluble proteins such as cytochrome c [23]. However, small polar head groups do not match large proteins because the charge distribution on the protein surface is often dispersed. This leads to random orientation along the SAM surface. Moreover, adsorption based on electrostatic interaction is affected by the solvent composition such as pH or ionic strength. The presence of excess ions, i.e., electrolyte, buffer molecules, detergent, etc., can mask the interaction between protein and surface-confined functional groups [24].

2.3. Surface-tethering of membrane proteins with protein tags

An immobilization strategy based on metal ion chelation provides a more specific and less accident-sensitive solution. Chelator-based immobilization is routine in chromatographic protein purification [25] where the interaction of oligo-histidine tags (His-tag) with di-valent metal ions immobilized via chelators such as nitrilo-triacetic acid (NTA) is exploited. His-tags comprise a sequence of six to twelve histidine residues which specifically bind to transition metals such as Cu(II), Co(II), Zn(II), or Ni(II) [26]. Recombinant proteins that carry a His-tag, are commonly generated by genetic engineering. The localization of the His-tag insertion can be arbitrarily chosen within the boundaries of genetic engineering and expression. The interaction between His-tag and Ni-NTA is much more specific than electrostatic interactions between protein and SAM surfaces.

Although the NTA-terminated thiol molecule can be synthesized prior to adsorption, it is inexpensive and simple to synthesize the immobilizing agent directly on the surface [27]. The coupling reaction is monitored in situ by SEIRA spectroscopy such that the chemical identity of the reaction products is instantly confirmed [28]. In the following, the sequence of steps towards a functional Ni-NTA SAM is presented and explained by the help of corresponding SEIRA spectra. In the first step, the hetero-bifunctional cross-linker dithiobis-succinimidylpropionate (DTSP) establishes a covalently bound thioadduct (thiosuccinimidylpropionate, TSP) with the gold surface. Once formed, the TSP monolayer shows characteristic bands at 1809, 1782, and 1739 cm^{-1}, which are assigned to the C=O stretching mode of the TSP ester group (Fig. 2(a)). After removal of unreacted DTSP, amino-nitrilotriacetic acid (ANTA) is introduced to the supernatant solution. The immobilized succinimidylester moiety of TSP reacts with the primary amine of ANTA to form a carboxamide linkage. The SEIRA spectrum (Fig. 2(b)) provides evidence for bond formation between TSP and ANTA. Differences were taken before and after the reaction, hence negative peaks represent the reactant species which is the ester group of TSP as lost in the coupling reaction. The reaction products (positive peaks) show characteristic bands of the carboxamide linkage (amide I at 1659 cm^{-1} and amide II at 1572 cm^{-1}) together with the unique bands of the carboxylate moieties (symmetric O-C-O stretching vibrations at 1404 cm^{-1}) that will coordinate the nickel ion in subsequent steps. As shown in this example, SEIRAS provides solid evidence for the formation of a NTA SAM layer atop the gold support.

After Ni^{2+} ions are added to the established NTA SAM, His-tagged proteins can be bound. We used detergent-solubilized, His-tagged cytochrome c oxidase (CcO) and monitored binding to the Ni-NTA SAM modified gold surface. The SEIRA spectrum in Fig. 2(c) shows the characteristic bands of α-helical proteins, namely amide I and II bands at 1660 cm^{-1} and 1550 cm^{-1}, respectively [29]. After removal of excess protein from the bulk solution, the amide I and amide II bands remain prominent in the spectrum. This indicates the formation of a tightly tethered protein layer on the solid-support gold surface.

The surface-tethered CcO still carries a "detergent belt" to saturate the hydrophobic part of the amphiphilic protein surface [30]. Bio-beads were added to the bulk solution to retract the detergent from the protein [31]. Lipids were supplied to replace the detergent and form a lipid layer that surrounds the CcO molecules (see Fig. 3 and [28]). The reconstitution of membrane proteins into lipids enhances the long-term stability of protein films. In our hands, lipid reconstituted monolayers of photosystem I [32] and of sensory rhodopsin II [33] are far more stable than detergent-solubilized protein layers.

Protein immobilization based on His-tag technology is highly versatile. However, the binding strength of the His-tag to monovalent NTA is just moderate (K_D in the order of 10^{-5}–10^{-6} M) [34]. The affinity for His-tags can be increased by bis-, and tris-NTA moieties [35]. The fact that His-tagged membrane proteins form stable solid-supported membranes on monovalent Ni-NTA modified surfaces is related to the lateral attraction among the membrane constituents. A disadvantage of the His-tag approach is the fact that proteins may contain histidine residues that are exposed to the protein surface which can lead to unspecific binding to the Ni-NTA moiety.

As an alternative to the His-tag/NTA approach, the streptavidin/biotin interaction can be exploited. Biotin exhibits an extremely high binding affinity to tetrameric streptavidin whose K_D of 10^{-15} M is considered to be the strongest non-covalent binding entity in nature [36]. Once a biotin modified gold surface has been generated by EDC catalyzed reaction with cysteamine, two of the four binding sites of streptavidin will be occupied by immobilized biotins while the other two are exposed to the bulk aqueous phase [37]. The latter are available for binding of strep-tagged proteins. The strep-tag is a peptide that binds to streptavidin at the same binding site as biotin.
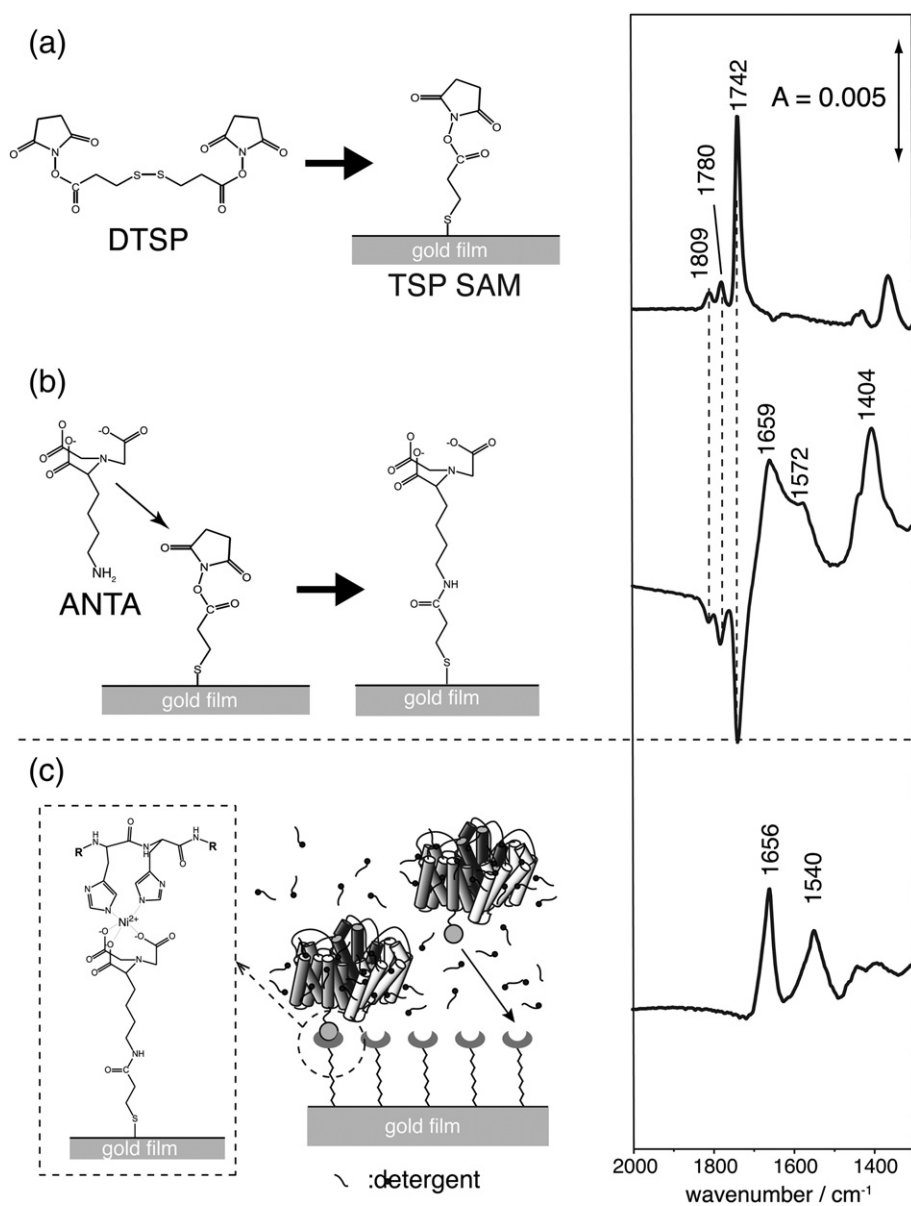
Fig. 2. Reaction sequence of surface modification (left), and in-situ recorded SEIRA spectra (right). (a) Self-assembly of the TSP monolayer on the bare Au surface after spontaneous splitting of the disulfide bond of DTSP. (b) Cross-linking of ANTA with the TSP monolayer. (c) Adsorption of cytochrome c oxidase monolayer on the Ni-NTA modified Au surface via the His-tag. From Ref. [17].
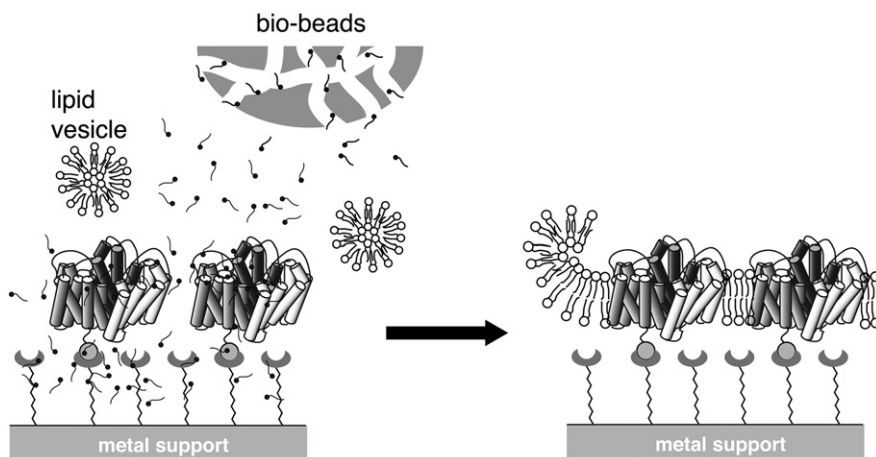

Fig. 3. Schematics of the lipid reconstitution of the surface-tethered membrane protein by detergent detraction by added Bio-beads.

As an example of this approach, the glutamate transporter *ecgltP* from *Escherichia coli* was tethered to a streptavidin/biotin-modified gold surface [37]. The obtained SEIRA spectra can clearly distinguish between streptavidin (amide I at 1673/1637 cm^{-1}) and *ecgltP* (amide I at 1659 cm^{-1}) because streptavidin owes a predominant β-sheet structure [38] while *ecgltP* is mainly composed of α-helices. The sensitive and qualitative distinction of adsorbed species is a unique advantage of SEIRAS in comparison to other surface techniques, such as Surface Plasmon Resonance (SPR) or Quartz Crystal Microbalance (QCM) that are restricted to quantitative information. The streptavidin/biotin method is superior to the His-NTA approach due to higher selectivity. However, the streptavidin tetramer has a high molecular mass (4 × 13 kDa) and forms a bulky layer along the plasmonic surface. This protein layer diminishes the effective amount of photons due to absorption in the fingerprint region. Furthermore, it forms a physical spacer on top of which bound species might not be probed with high sensitivity anymore. In this respect, the His-tag immobilization technique is advantageous.

2.4. Orientational control of surface-tethered proteins

The solid-supported membrane that has been established by the procedure presented above, offers acute control of protein orientation even for large proteins and protein complexes (Fig. 4 and [28]). Two CcO variants were expressed, each of which was modified with a His-tag on different subunits. One construct carried the tag at the C-terminus of subunit I (His-I) which faces the cytoplasm. The other variant had the His-tag on the C-terminus of subunit II (His-II), exposed to the periplasm. The periplasmic extension of subunit II harbors the docking site for redox partner cytochrome c. Since the His-tag binds specifically to Ni-NTA, CcO His-I was found to face the

Fig. 4. Solid-supported biomimetic membrane comprising a monolayer of oriented membrane protein embedded in a lipid bilayer (DMPC). (a) Cytochrome c oxidase (CcO) adsorbed to the Ni-NTA SAM layer via the His-tag at the C-terminus of subunit I (His-I). The binding site for cytochrome c is exposed towards the bulk solution. (b) CcO is oppositely oriented via binding of the His-tag at the C-terminus of subunit II (His-II). The binding site is inaccessible to cytochrome c due to the presence of the lipid bilayer. Bottom panel: SEIRA spectra of cytochrome c adsorption to the solid-supported CcO layer with (c) CcO oriented with the cytochrome c binding site facing the bulk solution as shown in (a), (d) the binding site oriented towards the solid surface (shown in (b)). From Ref. [26].

solid support with its cytoplasmatic side. When cytochrome c is added to the supernatant, CcO is able to receive electrons from the soluble heme protein as its binding site is exposed to the bulk solution (Fig. 4(a)). CcO His-II binds the Ni-NTA layer with its periplasmic side towards the gold surface (Fig. 4(b)). In this orientation, the binding site is not accessible to the bulk. Cytochrome c was added to the solution and binding was monitored by SEIRAS for both CcO His-I and His-II. Fig. 4(c) shows the recorded IR spectra during adsorption of cytochrome c to CcO oriented with the binding site towards the bulk solution (His-I). Two prominent bands at 1658 and 1550 cm^{-1} are assigned to the amide I and II vibrations of cytochrome c. When the same experiment was performed with CcO His-II construct, the characteristic amide bands of cytochrome c have not been observed (Fig. 4(d)). These results demonstrate that proteins whose activity critically depends on orientation, can only be probed in an experimental set-up that includes specific binding.

2.5. Nanodiscs: a variation of His-tag/Ni-NTA immobilization

Membrane proteins emerging from the ribosome must fold into stable three-dimensional structures of the cell membrane to accomplish their function. Living cells typically command a complex apparatus to control protein folding and membrane insertion. To study the folding process under controlled conditions, Sligar and coworkers introduced the so-called nanodiscs [39]. Nanodiscs are composed of small patches of lipid bilayer (10–20 nm in diameter) framed by an amphiphilic scaffold protein that shields the hydrophobic fatty acid chains from the aqueous buffer solution and inhibits spontaneous vesicle formation (Fig. 5). Nanodiscs serve as water-soluble carriers for membrane proteins and provide a native environment. As the scaffold protein is modified by a His-tag, oriented binding can be achieved. It is advantageous that the scaffold protein necessarily carries a His-tag but the target membrane protein is probed in its wild-type form.

Although nanodiscs are a promising platform to study membrane proteins, only Vogel and coworkers reported a SEIRAS application up to now [34]. They incorporated the G-protein-coupled receptor (GPCR) rhodopsin into nanodisc particles. 1.5 μM of rhodopsin-loaded nanodiscs (ca. 300 pmol of total molecules) was sufficient to clearly detect the amide bands at 1656 and 1550 cm^{-1} and a vibrational band from the lipid carbonyl at 1740 cm^{-1}. Photo-activity of rhodopsin was triggered by green light (530 nm) and light-minus-dark difference spectra were recorded. Absorbance changes in the SEIRA spectrum were in the range of 10^{-5} which proved to be sufficient to resolve band features indicative for changes in the chromophore and peptide conformation. Furthermore, the hydrogen-bond strength of mechanistically relevant amino acid side chains was probed and assigned.

3. Application of SEIRAS to functional studies of membrane proteins

The advantages of SEIRAS are most beneficial when applied to probe a protein monolayer. Protein function is triggered by external stimuli, such as light or chemicals. The use of the solid support as an electrode allows to apply a membrane potential or to directly inject electrons into the system. The combination of electrochemical methodologies with in situ vibrational spectroscopy provides new experimental opportunities to study the function of membrane proteins.

3.1. The redox-driven proton pump cytochrome c oxidase

After binding of His-tagged CcO to the gold surface, cytochrome c was introduced to the aqueous bulk solution [40]. The orientation of CcO was selected such that cytochrome c can specifically bind to the CcO monolayer (vide supra). Cyclic voltammetry was used to monitor the catalytic activity of CcO. Binding of cytochrome c is followed by
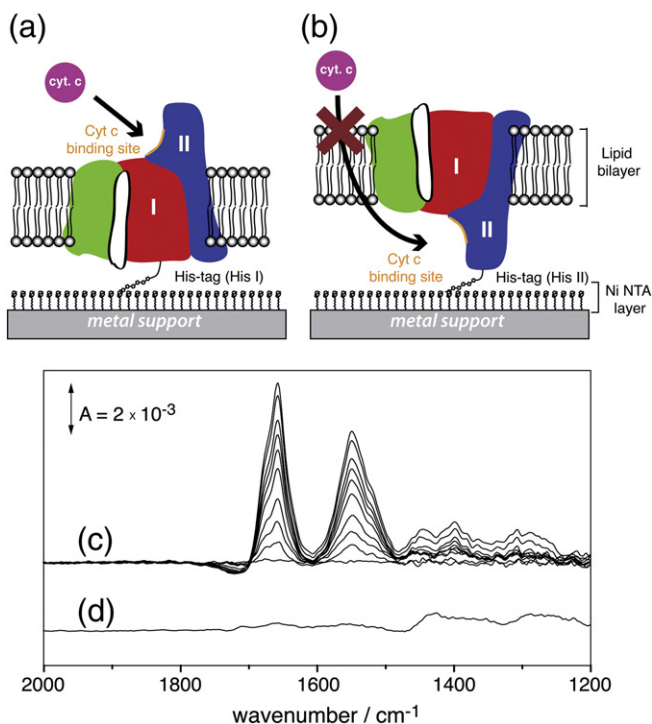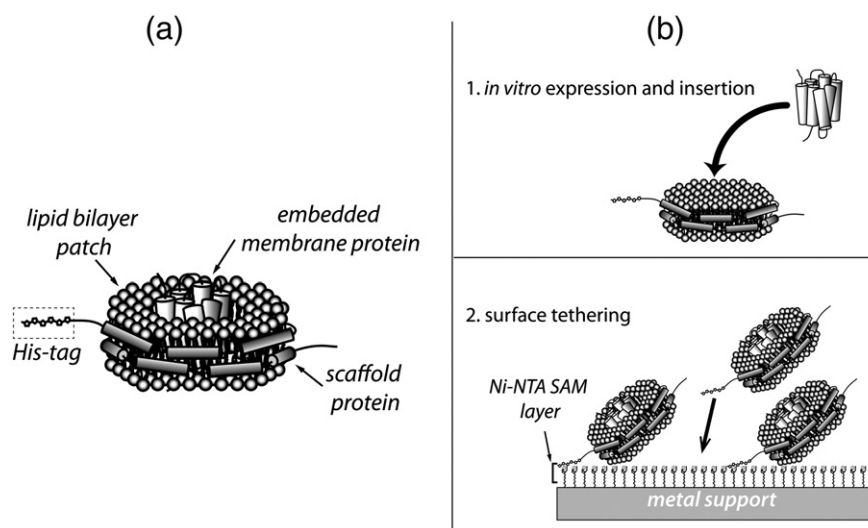
Fig. 5. (a) Membrane protein embedded in a nanodisc composed of lipid bilayer and membrane scaffold protein. (b) The membrane protein folds into the nanodisc during or after in-vitro expression. Then the protein/nanodisc is tethered to the Ni-NTA SAM modified surface via the His-tag at the terminus of the scaffold protein.

electron injection into the CcO catalytic center where dioxygen is reduced to water. A drastic increase in the reduction current was observed at potentials lower than $+260$ mV (vs. NHE) which is indicative of dioxygen reduction. Solid-supported CcO did not exhibit any electroactivity in the absence of cytochrome c. These results suggest that the surface-tethered CcO layer retains its catalytic properties. The preservation of protein functionality following monolayer formation is mandatory for meaningful studies and was demonstrated for other membrane proteins as well (vide infra).

Electrochemically induced IR difference spectroscopy has been performed on the functional cytochrome c/CcO complex. Spectra have been recorded while the potential was repeatedly increased and decreased (cyclic voltammetry). The resulting SEIRA spectra are remarkably similar to redox-induced difference spectra of cytochrome c in solution or when adsorbed to a carboxy-terminated SAM [23]. Thus, these bands emanate from conformational changes of cytochrome c induced by electrochemical oxidation when adsorbed to the CcO surface. It is remarkable that difference spectra of cytochrome c when adsorbed to SAMs equipped with different headgroups (hydroxyl, zwitterionic, or pyridine) exhibit different relative intensities. Only the carboxy-terminated surface provides similar redox-induced difference spectra of cytochrome c as if adsorbed to CcO. Thus, we concluded that the negatively charged carboxy-terminated SAM effectively mimics the (physiological) cytochrome c binding site of CcO which is dominated by negatively charged amino acid side chains (Asp and Glu).

3.2. Plant photosystems tethered to electrode surfaces for light energy conversion

In an attempt to generate a system for molecular studies on photobiological hydrogen production, the binding of His-tagged cyanobacterial photosystem II (PSII) to a Ni-NTA modified gold electrode was achieved and monitored by SEIRAS [41–44]. Bacterial PSII is a large protein complex comprising 20 subunits in total. Photosystem II represents the central unit in the light reaction of photosynthesis as it harbors the manganese complex to derive electrons from water and form molecular oxygen. Activity of surface-bound PSII was demonstrated by detecting a photocurrent upon illumination of the PSII monolayer. The variation in excitation wavelength produced an action spectrum that tallies with the absorption spectrum of chlorophyll. Thus, these experiments show that protein complexes as large as PSII can be assembled to the gold surface under preservation of its activity and probed on the level of a monolayer by SEIRAS.

Consequently, recombinant photosystem I (PSI) was attached to the gold electrode via the His-tag. Bacterial PSI owes twelve subunits with nine of these spanning the thylakoid membrane. Upon absorption of (red) light, it elevates electrons as derived from water splitting in PSII to highly reducing potentials. Three non-membrane subunits mediate the reduction of soluble PSI redox partners at the stroma-facing side of the membrane. As it has been discussed for CcO, PSI provides an interface for the interaction of soluble and membrane-bound proteins.

Light energy conversion into hydrogen requires the photosystem linked to a hydrogenase. The photoelectric effect generates electrons that are directed to the hydrogenase where protons are reduced to produce molecular hydrogen. Krassen et al. generated a construct of PSI and hydrogenase by first binding cyanobacterial PSI which had been deleted for the PsaE subunit ($PSI_{\Delta PsaE}$) via a His-tag that was attached to the periplasmic side of the membrane-integral PsaF subunit. This strategy allowed site-oriented attachment of the PSI variant to the electrode surface. The orientation was chosen to expose the PsaE binding site to the bulk solution.

Although the IR spectrum itself does not contain information of complex orientation, the authors were able to show that $PSI_{\Delta PsaE}$ did bind with the oxidizing side facing the gold film. Phenazonium methyl sulfate (PMS) was used as a diffusible electron mediator, taking up reducing equivalents from the gold surface at -90 mV (vs. NHE) and donating these to the P700 active site of PSI. Only for oriented binding and illumination around 680 nm, redox activity was recorded. Notably, light-dependent activity was found to be seven times more stable over time if $PSI_{\Delta PsaE}$ was reconstituted in lipids.

Not only did Krassen et al. immobilize PSI but couple the complex to a PsaE-hydrogenase chimera [45]. Hydrogenases are iron–sulphur enzymes that catalyze the uptake and production of molecular hydrogen close to the H^+/H_2 redox potential on platinum. While most hydrogenases display pronounced oxygen sensitivity, the authors made use of the oxygen-tolerant membrane-bound [NiFe] hydrogenase MBH of *Ralstonia eutropha* [46,47]. PsaE-MBH spontaneously binds the photosystem monolayer as PsaE sneaks into the vacant binding position of $PSI_{\Delta PsaE}$. The PsaE subunit brings the hydrogenase module into channeling distance to the distal PSI [4Fe–4S] cluster (F_B). In this arrangement, electrons get elevated at P700 upon light absorption, cross the PSI fold and reach the [NiFe] hydrogenase active site by tunneling from F_B to the proton-reducing MBH. The gold electrode reduces PMS which diffuses towards the oxidizing side of PSI to inject

an electron for another light-triggered elevation event. An increase in catalytic photocurrent pointed at an enhanced electron throughput of the PSI$_{\Delta PsaE}$ × PsaA-MBH monolayer and could be attributed to proton reduction by the hydrogenase. Finally, the rate of light-driven hydrogen evolution was determined by gas chromatography to 3.0 mmol H$_2$ h^{-1} per mg of chlorophyll. This high rate underlines the importance of improving electron transfer kinetics by coupling a hydrogenase to PSI.

The presented systems are highly relevant in terms of light energy conversion into biofuels of the third generation. The established system provides a unique platform to study and optimize the conversion of light energy into a stable chemical compound (here hydrogen), and SEIRAS provides the handle to track the underlying chemical conversions on the atomistic level.

3.3. Functional SEIRA spectroscopy

Functional changes in protein structure are addressed by IR difference spectroscopy in which the spectrum of a reference (resting) state is subtracted from the spectrum of an active state. The latter represents conditions as generated by triggering the activity of the protein via external stimuli. The resulting IR difference spectrum shows changes in band intensity and position. Consequently, only bands related to structural differences in the activated state appear in the spectra. By this procedure, it is possible to identify chemical groups that are involved in protein function. Over the past decades, FTIR difference spectroscopy successfully contributed to the elucidation of the reaction mechanism of many membrane proteins, in particular proton pumps and retinal proteins. As compared to IR spectroscopy on bulk protein samples, difference spectroscopy on a protein monolayer is technically very challenging.

3.3.1. Light-induced difference SEIRAS of sensory rhodopsin II

Sensory rhodopsin II from *Natronomonas pharaonis* (*Np*SRII) is the primary light sensor for negative phototaxis. The membrane protein is activated by blue–green light, propagates the signal to its transducer protein HtrII, and eventually triggers a modulation of flagella motion to escape the light [48]. The photo-reaction is initiated by absorption of visible light by the chromophore retinal, followed by protein conformational changes and the recovery of the resting state through several intermediate states.

Structural changes that follow photonic activation, have been investigated by difference SEIRAS. The recombinant protein was immobilized on a Ni-NTA SAM modified gold film electrode. Adsorption via the C-terminal His-tag of *Np*SRII resulted in an orientation with the extracellular surface facing the bulk aqueous solution [49]. After formation of the oriented monolayer, *Np*SRII was reconstituted in halobacterial lipids. Functional IR difference spectra between the ground (dark) state and the photo-stationary state (constant illumination with green light) were recorded by SEIRAS. Fig. 6 shows light difference spectra of the *Np*SRII monolayer as reconstituted in lipid bilayer (a) and solubilized in detergent (b). Negative bands refer to the dark state whereas positive bands correspond to the photo-stationary state. Prominent difference bands were assigned to the cofactor retinal plus amide II (1500–1600 cm^{-1}), amide I bands (1620–1680 cm^{-1}), and bands of carboxylic acid and various amide side chains (1690–1770 cm^{-1}) [50]. The spectra in Fig. 6(a) and (b) reveal distinct differences. Most prominent is the appearance of a negative band at 1544 cm^{-1} which can be assigned to the photo-isomerized retinal Schiff base. The disappearance of this band (negative peak), accompanied by a positive band at 1763 cm^{-1} suggests that the M-intermediate of the photocycle is predominating. The contribution at 1763 cm^{-1} was assigned to the primary proton acceptor aspartate 75. The ethylenic mode of the retinal (at 1550 cm^{-1}) is missing in the difference spectrum of lipid-reconstituted *Np*SRII suggesting that the predominating state is the

O intermediate. Differences in the two spectra are also noted in the amide I region. Together, these findings suggest that there are considerable differences in protein structure that critically depend on the immediate environment. The results reveal a structural influence of the lipid layer on protein function. Note that these differences had not been observed by conventional FTIR difference spectroscopy. Light-induced difference spectra of bulk *Np*SRII were reported to be invariant towards the described sample preparations [51].

3.3.2. Impact of the membrane potential on the photoreaction of SR II

The membrane potential is ubiquitous to all living cells. Yet, its impact on the conformation of membrane proteins has not been addressed by any biophysical technique with structural sensitivity. Like in the electrochemical experiments described above, the gold film can be used as the (working) electrode in a three-electrode configuration [33]. Since SR II is not redox active, the application of the electrode potential provides a voltage drop across the *Np*SRII monolayer through the Helmholtz double layer which mimics the cellular membrane potential. Fig. 7 depicts light-induced FTIR difference spectra of a *Np*SRII monolayer upon variation of the electrode potential from +0.6 to −0.8 V (pH 5.8). Apparently, drastic changes are induced with the onset at around −0.4 V. At E > −0.4 V, the observed bands display spectral features characteristic to the O intermediate. The overall spectrum in this potential range is not significantly altered except for the intensity of the 1757 cm^{-1} band which can be assigned to the C=O stretching mode of Asp75 (note that the band is detected at 1763 cm^{-1} in the M state, vide supra). The relative intensity of the Asp75 band is maximum at +0.2 V and decreases with the external potential shifting to more negative values. The decrease in band intensity suggests less protonated Asp75, hence a suppression of proton transfer from RSB to Asp75 in the O state. This result has been explained by the direction of the electric dipole in the external field and movement of the involved proton (Fig. 8). Since the adsorbed *Np*SRII is oriented with the extracellular side facing the bulk aqueous solution, internal proton transfer proceeds away from the electrode surface and towards the solution. When the electrode potential is set to values smaller +0.2 V, the net charge on the electrode surface becomes negative. An external electric field opposite to the direction of proton movement is induced. At large negative potentials, proton transfer to Asp75 is halted. This effect is specific for the transfer of the ion as the structural changes of the retinal cofactor and the protein backbone are largely unaffected by the external electric field. The latter is obvious from the invariance of the amide I band to the potential drop.

At E < −0.4 V, the entire spectral features resemble that of the M intermediate. Under constant illumination, photo-excited states accumulate at the level of the slowest, hence, rate-limiting intermediate state. Changes in the observed spectra at −0.4 V suggest that the O intermediate predominates at E > −0.4 V, while the M intermediate is rate-limiting for the photocycle at E < −0.4 V. This effect is explained in terms of a local pH shift at the membrane surface caused by charge compensation of the potential drop. When the potential is switched to very negative values (E < −0.4 V), the negative surface charge attracts counter ions to the electrode surface. In turn, the depletion of protons from the double layer causes a rise in surface pH of *Np*SRII [52]. This is likely due to the protonation state of surface residues at the extracellular side such as sensory Asp193. Asp193 is coupled to Asp75, the counter ion of the RSB. When deprotonation of Asp193 takes place for E < −0.4 V, interaction through the hydrogen-bonded network induces an increase of the pK$_a$ of Asp75 which drives proton translocation from the RSB to its counter ion resulting in the stabilization of the M intermediate. In summary, this experiment represents a unique example of monitoring the effect of the membrane potential on the functionality of a membrane protein. SEIRAS is a unique method that reports atomistic information
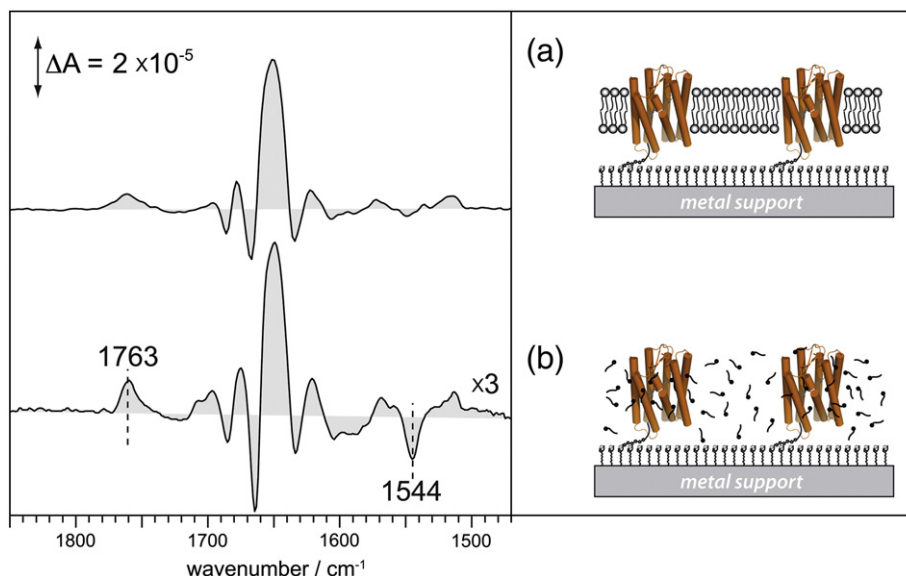
Fig. 6. Light-induced SEIRA difference spectra of a monolayer of sensory rhodopsin II from *N. pharaonis* with (a) reconstituted in halobacterial polar lipids, and (b) solubilized in detergent.

about the influence of the membrane potential on the functional changes of a membrane protein.

4. Perspective

It has been almost 20 years since SEIRAS appeared as a surface analytical method but the use of SEIRAS for functional studies of proteins has been introduced only during the last decade. Since then, the number of applications increased rapidly. Improvements in

Fig. 7. Light-induced SEIRA difference spectra of a monolayer of sensory rhodopsin II in the presence of an externally applied electrical potential. Difference spectra were recorded between the dark and light states under continuous illumination with blue–green light ($\lambda_{max} = 500$ nm). The electrode potential was varied in the range between +0.6 and −0.8 V (vs. NHE = Normal Hydrogen Electrode). From Ref. [39].

specific and effective tethering of proteins to the plasmonic substrate helped to mature the methodology. The full range of possible SEIRAS applications is beyond the scope of this review and several attractive examples such as *in-situ* monitoring of DNA hybridization [53] or trace sensor for immunoassays [54] have not been introduced here. In the final chapter, we will showcase applications of SEIRAS to complex cellular systems.

One of the ultimate goals of biological FTIR spectroscopy is to probe living cells. The overwhelming mixture of spectral contributions from a variety of different proteins, lipids, sugars, nucleic acids, and other biological components are expected to generate an intricate IR spectrum of the intact biological cell. Despite this obstacle, Busalmen et al. [55,56] succeeded to record SEIRA spectra of the electrogenic proteobacterium *Geobacter sulfurreducens*. These peculiar Fe(III)-reducing bacteria live in an environment deficient of oxygen. They are capable to harvest electrons directly from soil metal in
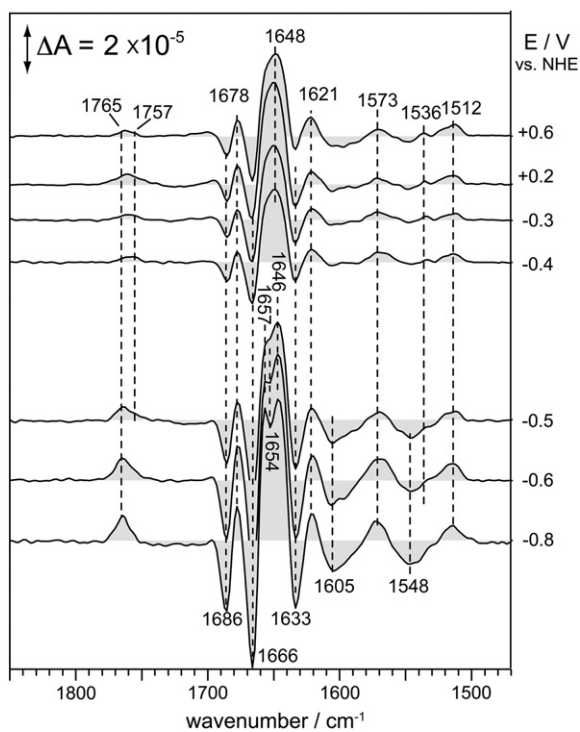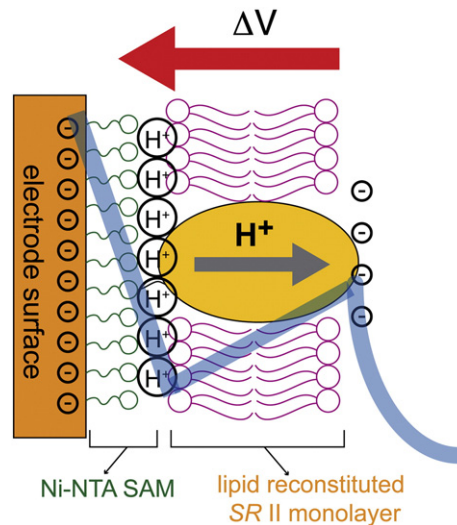

Fig. 8. Sketch of the protein monolayer at the solid liquid interface immersed in the electrochemical double layer. The local potential profile is denoted by blue dashed line. The bold red arrow indicates the direction of the net electric fields created by the potential difference between the electrode surface and the bulk electrolyte. The gray arrow represents proton translocation after photo-excitation of the protein.

order to oxidize organic compounds. This is due to the redox activity of a large number of c-type cytochromes in the outer membrane of *G. sulfurreducens*. Busalmen et al. attached these bacteria directly to the SEIRA-active gold surface and observed metal-reducing activity when the electrode was set to the typical redox potential of cytochrome c. The observed SEIRA spectra revealed major spectral changes that are similar to those of isolated cytochrome c. The selective observation of the cell membrane owes to the optical near-field effect of SEIRAS. Only compounds in the vicinity of the gold surface are 'visible' to SEIRA spectroscopy — the cytoplasm cannot be probed. The recorded spectra may still be too complicated to help elucidating the mechanisms of bacterial activities. Still, this work represents a unique application of SEIRAS to living matter.

Another interesting application is the combination of SEIRAS with Scanning Near-field Optical Microscopy (SNOM). Although vibrational spectroscopy can probe samples down to the monolayer level, lateral resolution is usually limited by diffraction (~5 μm for mid-IR). This limit was overcome by the invention of near-field proximal probes. In the so-called scattering type Scanning Near-field Infrared Microscopy (s-SNIM), high spatial resolution is achieved by an "apertureless" tip, a sharp metallic needle commonly used in Atomic Force Microscopy (AFM). The function of the metallic needle is that of an optical antenna that provides a strong electric field at its apex upon IR irradiation, equivalent to the near-field effect of the gold island structures used in SEIRAS. The strong field at the tip has a transverse width that corresponds to the radius of the tip curvature. The lateral microscopic resolution is currently at about 10–20 nm. Recently, Ballout et al. [57] reported the application of SNIM to surface-tethered CcO embedded in a lipid bilayer. The authors scanned the nanoscale topography and recorded near-field IR images as a function of frequency between 1600 cm^{-1} and 1800 cm^{-1}. By analyzing the correlation between height and near-field contrast, the distribution of proteins and lipids was mapped out.

The sensitivity of SEIRAS must be increased in the future to be able to detect the extremely small bands in a reaction-induced difference spectrum. The absorbance changes in difference spectra of protein monolayers are typically in the order of 10^{-5}–10^{-6} [33]. This range can only be attained when the surface is densely covered by fully functional protein. Adato et al. achieved IR signal enhancement in the range of 10^4–10^5 by precise control of size, shape, and geometry of the gold nanoparticles [15]. This factor is 10^2–10^3 times higher than for conventional gold surfaces used in SEIRAS. A drawback of this method is the precise and controlled assembly of gold nanoparticles on the surface. Special equipments for surface assembly are required to achieve such large enhancement. A two-layer gold surface proposed by Nowak et al. represents a more practical approach to enhance the electromagnetic field [58]. The authors reported a six times larger enhancement than that of SEIRAS on a conventional gold surface. The application of new IR sources, such as the intense and tunable mid-infrared emission of quantum cascade lasers (QCLs, [59,60]), represents another means to improve the sensitivity. As the signal-to-noise ratio in IR spectroscopy is typically shot-noise limited with high sensitivity detectors, the high emission power of QCL (>400 mW) leads to higher sensitivity. The strong emission from QCLs can also be exploited to perform ATR/SEIRAS experiments with multiple reflections. In conventional ATR/SEIRAS, the weak emission from the globar is strongly attenuated by coupling the IR emission into the plasmonic absorption of the gold film and a single reflection is typically used for probing. Multi-reflection ATR offers the advantage to observe stronger absorbance by the sample due to the multiple points that the radiation is interacting with.

In conclusion, there is plenty of space for SEIRAS to improve as an analytical tool for biological samples. Still, SEIRAS is superior to other modern surface spectroscopic techniques like e.g. sum frequency generation (SFG [61]), tip-enhanced vibrational spectroscopy (TERS [62,63]) and SNIM ([57]) as it is fairly simple in optical design. In

the end, SEIRAS yields IR spectra of single biomembranes with superb signal-to-noise and reasonable cost-to-performance ratio.

Acknowledgements

References

[1] R. Vogel, F. Siebert, Vibrational spectroscopy as a tool for probing protein function, Curr. Opin. Chem. Biol. 4 (2000) 518–523.

[2] A. Kawanabe, H. Kandori, Photoreactions and structural changes of *Anabaena* sensory rhodopsin, Sensors-Basel 9 (2009) 9741–9804.

[3] C. Berthomieu, R. Hienerwadel, Fourier transform infrared (FTIR) spectroscopy, Photosynth. Res. 101 (2009) 157–170.

[4] I. Radu, M. Schleeger, C. Bolwien, J. Heberle, Time-resolved methods in biophysics. 10. Time-resolved FT-IR difference spectroscopy and the application to membrane proteins, Photochem. Photobiol. Sci. 8 (2009) 1517–1528.

[5] C. Kotting, J. Guldenhaupt, K. Gerwert, Time-resolved FTIR spectroscopy for monitoring protein dynamics exemplified by functional studies of Ras protein bound to a lipid bilayer, Chem. Phys. 396 (2012) 72–83.

[6] J.M. Chalmers, P.R. Griffiths, Handbook of Vibrational Spectroscopy, J. Wiley, New York, 2002.

[7] M. Osawa, K. Ataka, K. Yoshii, Y. Nishikawa, Surface-enhanced infrared-spectroscopy — the origin of the absorption enhancement and band selection rule in the infrared-spectra of molecules adsorbed on fine metal particles, Appl. Spectrosc. 47 (1993) 1497–1502.

[8] M. Frasconi, F. Mazzei, T. Ferri, Protein immobilization at gold-thiol surfaces and potential for biosensing, Anal. Bioanal. Chem. 398 (2010) 1545–1564.

[9] F. Neubrech, A. Pucci, T.W. Cornelius, S. Karim, A. Garcia-Etxarri, J. Aizpurua, Resonant plasmonic and vibrational coupling in a tailored nanoantenna for infrared detection, Phys. Rev. Lett. 101 (2008).

[10] M. Osawa, M. Kuramitsu, A. Hatta, W. Suetaka, Electromagnetic effect in enhanced infrared-absorption of adsorbed molecules on thin metal-films, Surf. Sci. 175 (1986) L787–L793.

[11] M. Osawa, K. Ataka, Electromagnetic mechanism of enhanced infrared-absorption of molecules adsorbed on metal island films, Surf. Sci. 262 (1992) L118–L122.

[12] Y. Nishikawa, T. Nagasawa, K. Fujiwara, M. Osawa, Silver island films for surface-enhanced infrared-absorption spectroscopy — effect of island morphology on the absorption enhancement, Vib. Spectrosc. 6 (1993) 43–53.

[13] M. Osawa, K. Ataka, K. Yoshii, T. Yotsuyanagi, Surface-enhanced infrared Atr spectroscopy for in-situ studies of electrode–electrolyte interfaces, J. Electron. Spectrosc. 64–5 (1993) 371–379.

[14] A. Pucci, F. Neubrech, D. Weber, S. Hong, T. Toury, M.L. de la Chapelle, Surface enhanced infrared spectroscopy using gold nanoantennas, Phys. Status Solidi. B 247 (2010) 2071–2074.

[15] R. Adato, A.A. Yanik, J.J. Amsden, D.L. Kaplan, F.G. Omenetto, M.K. Hong, S. Erramilli, H. Altug, Ultra-sensitive vibrational spectroscopy of protein monolayers with plasmonic nanoantenna arrays, Proc. Natl. Acad. Sci. U. S. A. 106 (2009) 19227–19232.

[16] A. Bewick, K. Kunimatsu, Infrared-spectroscopy of the electrode–electrolyte interphase, Surf. Sci. 101 (1980) 131–138.

[17] W. Suetaka, Surface Infrared and Raman Spectroscopy, Methods and Application, Plenum Press, 1995.

[18] W.G. Golden, K. Kunimatsu, H. Seki, Application of polarization-modulated Fourier-transform infrared reflection absorption-spectroscopy to the study of carbon-monoxide adsorption and oxidation on a smooth platinum-electrode, J. Phys. Chem. 88 (1984) 1275–1277.

[19] K. Kunimatsu, R.O. Lezna, M. Enyo, Adsorption and oxidation of carbon-monoxide on a rhodium electrode studied by in situ infrared-spectroscopy, J. Electroanal. Chem. 258 (1989) 115–126.

[20] J. Guldenhaupt, Y. Adiguzel, J. Kuhlmann, H. Waldmann, C. Kotting, K. Gerwert, Secondary structure of lipidated Ras bound to a lipid bilayer, FEBS J. 275 (2008) 5910–5918.

[21] P. Pinkerneil, J. Guldenhaupt, K. Gerwert, C. Kotting, Surface-attached polyhistidine-tag proteins characterized by FTIR difference spectroscopy, ChemPhysChem 13 (2012) 2649–2653.

[22] R.M. Nyquist, K. Ataka, J. Heberle, The molecular mechanism of membrane proteins probed by evanescent infrared waves, ChemBioChem 5 (2004) 431–436.

[23] K. Ataka, J. Heberle, Functional vibrational spectroscopy of a cytochrome c monolayer: SEIDAS probes the interaction with different surface-modified electrodes, J. Am. Chem. Soc. 126 (2004) 9445–9457.

[24] L.J.C. Jeuken, Conformational reorganisation in interfacial protein electron transfer, Biochem. Biophys. Acta 1604 (2003) 67–76.

[25] H. Block, B. Maertens, A. Spriestersbach, N. Brinker, J. Kubicek, R. Fabis, J. Labahn, F. Schafer, Immobilized-metal affinity chromatography (IMAC): a review, Meth. Enzymol. 463 (2009) 439–473.

[26] V. Gaberc-Porekar, V. Menart, Potential for using histidine tags in purification of proteins at large scale, Chem. Eng. Technol. 28 (2005) 1306–1314.

[27] G.T. Hermanson, Bioconjugate Techniques, Academic Press, San Diego, 1996.

[28] K. Ataka, F. Giess, W. Knoll, R. Naumann, S. Haber-Pohlmeier, B. Richter, J. Heberle, Oriented attachment and membrane reconstitution of His-tagged cytochrome c

oxidase to a gold electrode: in situ monitoring by surface-enhanced infrared absorption spectroscopy, J. Am. Chem. Soc. 126 (2004) 16199–16206.

[29] S. Krimm, J. Bandekar, Vibrational spectroscopy and conformation of peptides, polypeptides, and proteins, Adv. Prot. Chem. 38 (1986) 181–364.

[30] E. Pebay-Peyroula, R.M. Garavito, J.P. Rosenbusch, M. Zulauf, P.A. Timmins, Detergent structure in tetragonal crystals of OmpF porin, Structure 3 (1995) 1051–1059.

[31] J.L. Rigaud, D. Levy, G. Mosser, O. Lambert, Detergent removal by non-polar polystyrene beads — applications to membrane protein reconstitution and two-dimensional crystallization, Eur. Biophys. J. 27 (1998) 305–319.

[32] H. Krassen, S. Ott, J. Heberle, In vitro hydrogen production-using energy from the sun, Phys. Chem. Chem. Phys. 13 (2011) 47–57.

[33] X. Jiang, M. Engelhard, K. Ataka, J. Heberle, Molecular impact of the membrane potential on the regulatory mechanism of proton transfer in sensory rhodopsin II, J. Am. Chem. Soc. 132 (2010) 10808–10815.

[34] E. Zaitseva, M. Saavedra, S. Banerjee, T.P. Sakmar, R. Vogel, SEIRA spectroscopy on a membrane receptor monolayer using lipoprotein particles as carriers, Biophys. J. 99 (2010) 2327–2335.

[35] S. Lata, A. Reichel, R. Brock, R. Tampe, J. Piehler, High-affinity adaptors for switchable recognition of histidine-tagged proteins, J. Am. Chem. Soc. 127 (2005) 10205–10215.

[36] N.M. Green, Avidin .3. Nature of biotin-binding site, Biochem. J. 89 (1963) 599–609.

[37] X. Jiang, A. Zuber, J. Heberle, K. Ataka, In situ monitoring of the orientated assembly of strep-tagged membrane proteins on the gold surface by surface enhanced infrared absorption spectroscopy, Phys. Chem. Chem. Phys. 10 (2008) 6381–6387.

[38] S. Freitag, I. LeTrong, L. Klumb, P.S. Stayton, R.E. Stenkamp, Structural studies of the streptavidin binding loop, Protein Sci. 6 (1997) 1157–1166.

[39] T.H. Bayburt, Y.V. Grinkova, S.G. Sligar, Self-assembly of discoidal phospholipid bilayer nanoparticles with membrane scaffold proteins, Nano. Lett. 2 (2002) 853–856.

[40] K. Ataka, B. Richter, J. Heberle, Orientational control of the physiological reaction of cytochrome c oxidase tethered to a gold electrode, J. Phys. Chem. B. 110 (2006) 9339–9347.

[41] A. Badura, B. Esper, K. Ataka, C. Grunwald, C. Woll, J. Kuhlmann, J. Heberle, M. Rögner, Light-driven water splitting for (bio-)hydrogen production: photosystem 2 as the central part of a bioelectrochemical device, Photochem. Photobiol. 82 (2006) 1385–1390.

[42] A. Badura, D. Guschin, B. Esper, T. Kothe, S. Neugebauer, W. Schuhmann, M. Rögner, Photo-induced electron transfer between photosystem 2 via cross-linked redox hydrogels, Electroanalysis 20 (2008) 1043–1047.

[43] A. Badura, D. Guschin, T. Kothe, M.J. Kopczak, W. Schuhmann, M. Rögner, Photo-current generation by photosystem 1 integrated in crosslinked redox hydrogels, Energy Environ. Sci. 4 (2011) 2435–2440.

[44] A. Badura, T. Kothe, W. Schuhmann, M. Rögner, Wiring photosynthetic enzymes to electrodes, Energy Environ. Sci. 4 (2011) 3263–3274.

[45] H. Krassen, A. Schwarze, B. Friedrich, K. Ataka, O. Lenz, J. Heberle, Photosynthetic hydrogen production by a hybrid complex of photosystem I and [NiFe]-hydrogenase, ACS Nano. 3 (2009) 4055–4061.

[46] G. Goldet, A.F. Wait, J.A. Cracknell, K.A. Vincent, M. Ludwig, O. Lenz, B. Friedrich, F.A. Armstrong, Hydrogen production under aerobic conditions by membrane-bound hydrogenases from Ralstonia species, J. Am. Chem. Soc. 130 (2008) 11106–11113.

[47] M. Ludwig, J.A. Cracknell, K.A. Vincent, F.A. Armstrong, O. Lenz, Oxygen-tolerant H-2 oxidation by membrane-bound [NiFe] hydrogenases of Ralstonia species. Coping with low level H-2 in air, J. Biol. Chem. 284 (2009) 465–477.

[48] W.D. Hoff, K.H. Jung, J.L. Spudich, Molecular mechanism of photosignaling by archaeal sensory rhodopsins, Ann. Rev. Bio. Phys. BioMol. Struct. 26 (1997) 223–258.

[49] X. Jiang, E. Zaitseva, M. Schmidt, F. Siebert, M. Engelhard, R. Schlesinger, K. Ataka, R. Vogel, J. Heberle, Resolving voltage-dependent structural changes of a membrane photoreceptor by surface-enhanced IR difference spectroscopy, Proc. Natl. Acad. Sci. U. S. A. 105 (2008) 12113–12117.

[50] M. Engelhard, B. Scharf, F. Siebert, Protonation changes during the photocycle of sensory rhodopsin II from Natronobacterium pharaonis, FEBS Lett. 395 (1996) 195–198.

[51] Y. Furutani, M. Iwamoto, K. Shimono, N. Kamo, H. Kandori, FTIR spectroscopy of the M photointermediate in pharaonis phoborhodopsin, Biophys. J. 83 (2002) 3482–3489.

[52] M. Iwamoto, Y. Furutani, Y. Sudo, K. Shimono, H. Kandori, N. Kamo, Role of Asp193 in chromophore-protein interaction of pharaonis phoborhodopsin (sensory rhodopsin II), Biophys. J. 83 (2002) 1130–1135.

[53] J.Y. Xu, B. Jin, Y. Zhao, K. Wang, X.H. Xia, In situ monitoring of the DNA hybridization by attenuated total reflection surface-enhanced infrared absorption spectroscopy, Chem. Commun. 48 (2012) 3052–3054.

[54] C.W. Brown, Y. Li, J.A. Seelenbinder, P. Pivarnik, A.G. Rand, S.V. Letcher, O.J. Gregory, M.J. Platek, Immunoassays based on surface enhanced infrared absorption spectroscopy, Anal. Chem. 70 (1998) 2991–2996.

[55] J.P. Busalmen, A. Berna, J.M. Feliu, Spectroelectrochemical examination of the interaction between bacterial cells and gold electrodes, Langmuir 23 (2007) 6459–6466.

[56] J.P. Busalmen, A. Esteve-Nunez, A. Berna, J.M. Feliu, ATR-SEIRAS characterization of surface redox processes in G. sulfurreducens, Bioelectrochemistry 78 (2010) 25–29.

[57] F. Ballout, H. Krassen, I. Kopf, K. Ataka, E. Brundermann, J. Heberle, M. Havenith, Scanning near-field IR microscopy of proteins in lipid bilayers, Phys. Chem. Chem. Phys. 13 (2011) 21432–21436.

[58] C. Nowak, C. Luening, W. Knoll, R.L.C. Naumann, A two-layer gold surface with improved surface enhancement for spectro-electrochemistry using surface-enhanced infrared absorption spectroscopy, Appl. Spectrosc. 63 (2009) 1068–1074.

[59] J. Faist, F. Capasso, D.L. Sivco, C. Sirtori, A.L. Hutchinson, A.Y. Cho, Quantum cascade laser, Science 264 (1994) 553–556.

[60] M. Brandstetter, A. Genner, K. Anic, B. Lendl, Tunable external cavity quantum cascade laser for the simultaneous determination of glucose and lactate in aqueous phase, Analyst 135 (2010) 3260–3265.

[61] Y.W. Liu, J. Jasensky, Z. Chen, Molecular interactions of proteins and peptides at interfaces studied by sum frequency generation vibrational spectroscopy, Langmuir 28 (2012) 2113–2121.

[62] T. Deckert-Gaudig, V. Deckert, Nanoscale structural analysis using tip-enhanced Raman spectroscopy, Curr. Opin. Chem. Biol. 15 (2011) 719–724.

[63] T. Deckert-Gaudig, R. Bohme, E. Freier, A. Sebesta, T. Merkendorf, J. Popp, K. Gerwert, V. Deckert, Nanoscale distinction of membrane patches — a TERS study of Halobacterium salinarum, J. Biophotonics 5 (2012) 582–591.